inter.noise
HAMBURG 2016

Statistical-Empirical Modelling of Aerofoil Noise and Performance Subjected to Leading Edge Serrations

Till BIEDERMANN[1]; Tze Pei CHONG[2]; Frank KAMEIER[1]

[1] University of Applied Sciences Dusseldorf, Germany

[2] Brunel University London, UK

ABSTRACT

Sinusoidal leading edge serrations of a cambered NACA65(12)-10 aerofoil were analysed with the aim of reducing leading edged broadband noise emissions due to aerofoil-gust-interaction in a high turbulent flow. A statistical-empirical model was developed to quantify the main effect as well as the interdependencies of flow and design parameters on the noise reduction capability of serrated leading edges. Apart from the main effects, significant interdependencies of turbulence intensity and serration wavelength were observed, validated and quantified. Aeroacoustic findings are complemented by visualisation of the aerodynamic flow pattern via particle image velocimetry for selected leading edge configurations in order to deepen the understanding of the underlying noise reduction mechanisms. It was observed that a noise reduction is accompanied by a reduction of the turbulence intensity within the serration although it could be shown that this effect is mainly attributed to an altering mean velocity distribution. Moreover, numerical studies were conducted to enable predictions of the aerodynamic performance in terms of lift and drag of the serrated leading edges with the objective to define a multi-optimum of noise reduction and performance.

Keywords: Passive Noise Control, Leading Edge Serrations, Aerofoil-Gust-Interaction-Noise
I-INCE Classification of Subjects Numbers: 21.6.3, 21.6.4, 75.1, 13.1.5

1. INTRODUCTION

Recent research has firmly established sinusoidal leading edge (LE) serrations as an effective passive treatment to reduce the emitted broadband noise of an aerofoil exposed to a highly turbulent flow. A reduction in the overall sound pressure level of up to ΔOASPL = 7dB and local sound pressure level reductions above ΔSPL = 10dB in the relevant frequency region could be reached (1–4). Several parameters have been found to influence the effectiveness of noise reduction by leading edge (LE) serrations, which include the Reynolds number (Re), turbulence intensity (Tu), serration amplitude (A/C), serration wavelength (λ/C) and angle of attack (AoA). However, up to now, these parameters have been regarded independently, and only little effort was made to analyse them as an interrelated system of factors with respect to the noise reduction. This serves as motivation for the current work, where a comprehensive statistical-empirical model has been developed with the aim to describe the noise emittance and reduction of serrated LE as an interrelated system of several influencing parameters (Chapter 3).

Although different hypotheses on the noise reduction mechanism were proposed before, they have hitherto not been comprehensively verified. In general, three mechanisms have been identified that could be responsible for the reduction in broadband noise. First is the effect of reduced spanwise correlation coefficients as a result of incoherent response times of the incoming turbulence; second, a reduction of the acoustic sources as manifested in the reduction in RMS pressure fluctuation at the serration peak; and, third, a reduction of the streamwise turbulence intensity due to the converging flow within the serrations (5,6). Up to now, research on the effect of LE serrations either focussed on the noise reduction capability or on the aerodynamic advantages/disadvantages of the performance of serrated aerofoils itself. In doing so, two important features of LE serrations remain unattended.

[1] till.biedermann@hs-duesseldorf.de
[2] t.p.chong@brunel.ac.uk

First, the possibility of concluding on the noise reduction mechanisms by analysing the flow patterns in front and within the interstices of the serrations. In general, the incoming turbulence amplifies the surface pressure fluctuations close to the aerofoil LE, which then radiate into broadband noise (7,8). The serrated LEs, on the other hand, cause a significant decrease in the surface pressure fluctuations and subsequently reduce the broadband noise level. To visualise the effect of the serrations on the incoming gust was the aim of the currently carried out PIV study (Chapter 4). Although the aeroacoustic and aerodynamic experiments were carried out independently, the results are supplementary to each other where a causal relationship between the flow patterns and the aeroacoustic results for a selected LE configuration is established (9).

Second is the possibility to regard the noise reduction capability and the aerodynamic performance as an interrelated system in order to rate this application with regard to real-life implementation. The humpback whale inspired LE serrations are believed to be an effective noise reduction technology in rotating machines such as at the guide vanes of axial fans or as rotor-applications at contra-rotating open rotors (CROR) or ceiling fans. In order to get to know the aerodynamic performance, rudimentary numerical studies were carried out and are presented in Chapter 5.

2. EXPERIMENTAL SETUP

2.1 Analysed Aerofoils

In the current study, a cambered NACA65(12)-10 aerofoil was utilised due to its similarity to real-life application such as the stator vanes or axial fan blades. As shown in Fig. 1, the aerofoil has a chord length of C = 150 mm and a span width of S = 300 mm. Between the leading edge (x/C = 0) and x/C = 0.3, there is a section that can be removed and replaced by different serration profiles. Note that x is the streamwise direction. Further downstream, 0.3 < x/C < 1.0, is the unmodified aerofoil main body. Once attached, the serrations form a continuous profile giving the appearance that they are cut into the main body of the aerofoil. The serration geometry is defined by two parameters: amplitude (chordwise peak-to-trough value) and wavelength (spanwise peak-to-peak-value). Both parameters are normalised by the aerofoil chord length C = 150 mm. The angle of attack is defined as a non-dimensional ratio of vertical LE tip displacement (z) and the height of the nozzle outlet (H). The shape of the LE serrations is designed according to a sinusoidal curve, and the NACA65(12)-10 profile was extruded along the line of this curve.

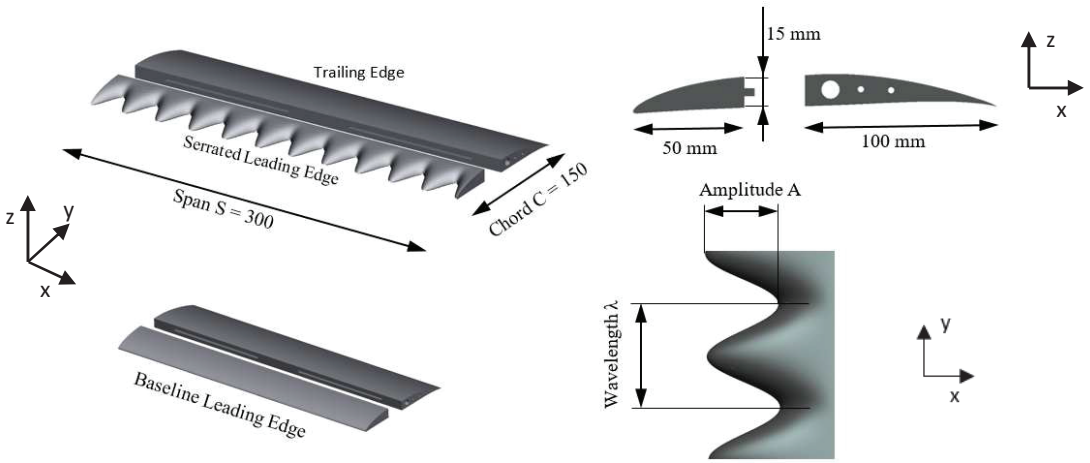

Figure 1 – Normalised NACA65(12)-10 aerofoil main body and re-attachable leading edge with measures of importance for the acoustical treatment in the open jet stream.

2.2 Grid Generated Turbulence

Experiments were conducted in the aeroacoustics facility at *Brunel University London* where an open jet wind tunnel is situated in a 4 m x 5 m x 3.4 m semi-anechoic chamber (10). The nozzle exit is rectangular with dimensions of 0.10 m (height) x 0.30 m (width). In order to achieve high turbulence intensities (Tu), grids of various spacing were used. Adopting the criteria set by *Laws* and *Livesey* (11), all grids are biplane square meshes with a constant ratio of bar diameter and mesh size (M/d = 5). Five different grids for the generation of Tu in the range of 2.1 % ≤ Tu ≤ 5.5 % were defined and verified experimentally.

The turbulence intensity near the aerofoil's LE is assumed isotropic. In this context, the analysis of the measured turbulence energy spectra showed a good agreement with the turbulence model (Fig. 2) of *Liepmann* in Eq. (1), after having applied the correction function of *Rozenberg* (12) in Eq. (2) in order to take the dilution in the high-frequency region close to the Kolmogorov scale into account. ($\overline{u'^2}$) is the velocity fluctuation, Λ_{uu} is the integral length scale, K_x the streamwise wave number and K_η a constant that controls the gradient of the roll off at high frequencies.

$$\Phi_{uu}^{L}(\omega) = {\overline{u'^2}\Lambda_{uu}}/{\pi U_0} \cdot {1}/{1 + K_x^2 {\Lambda_{uu}}^2} \tag{1}$$

$$G_{Kolm.} = exp\left(\left({-9}/{4}\right) \cdot \left({K_x}/{K_\eta}\right)^2\right) \tag{2}$$

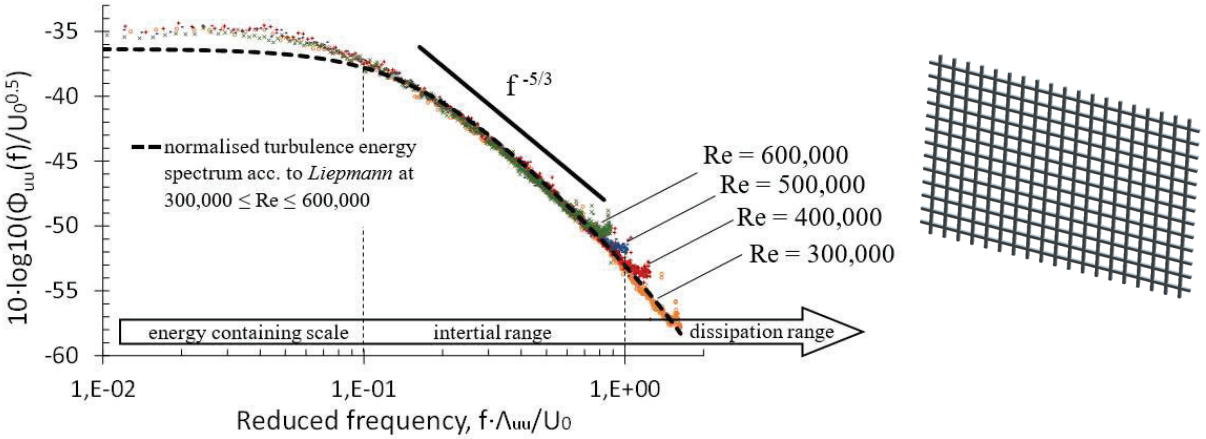

Figure 2 – Normalised turbulence energy spectrum according to *Liepmann* at $30ms^{-1} \leq U0 \leq 60ms^{-1}$, Tu = 3.9%, measured at the imaginary location of the aerofoil leading edge. Applied correction for high-frequency dilution according to *Rozenberg*.

2.3 Analysed Parameters

Prior to the modelling, recent scientific output was screened in order to identify meaningful target values for the present study. According to Table 1, the influence of five different parameters on the noise radiation and reduction was analysed, namely the Reynolds number (Re), the turbulence intensity (Tu, Eq.3), the serration amplitude (A/C) and the wavelength (λ/C) as well as the angle of attack (z/H). The Reynolds number is based on the aerofoil chord length, where the turbulence intensity is based on the streamwise velocity component [u].

$$Tu(u) = {\sqrt{u'^2}}/{\overline{U}} \tag{3}$$

In order to produce a sufficient data pool, each parameter was varied on five levels, where the settings between the minimum and maximum values were given by the applied modelling technique of *Design of Experiments* (DoE). In addition to the serrated cases, all measurements were repeated with a straight LE to serve as the baseline case in order to define the absolute noise reduction. Free field measurements of the AGI-Noise (Aerofoil-Gust-Interaction) were conducted in the aeroacoustic facility at *Brunel University London* (10). The aerofoil was held by side plates and attached flushed to the nozzle lips. Noise measurements at the aeroacoustic wind tunnel were made by a PCB ½-inch prepolarised ICP® condenser microphone at polar angles of 90 degree at a distance of 0.95 m from the LE of the aerofoil at mid-span. The acoustic data was recorded at a sampling rate of SR = 40 kHz, with a block size of BZ = 1024. The feasible frequency range for the data analyses was set to 300 Hz $\leq f_{Analyse} \leq$ 10 kHz, where the lower limit is due to the cut-off frequency of the anechoic chamber. The upper limit was chosen in order to avoid the possible influences by aerofoil self-noise, which is not related to aerofoil-gust-interaction. The range of jet speeds under investigation is between 25 ms^{-1} and 60 ms^{-1}, corresponding to Reynolds' numbers based on the aerofoil chord length of $2.5 \cdot 10^5 \leq Re \leq 6 \cdot 10^5$ respectively.

Table 1 – Non-dimensional DoE (Design of Experiments) levels of the different factors of interest. Serration amplitude and wavelength normalised by aerofoil chord (C = 150 mm); angle of attack normalised by nozzle height (H = 100 mm).

	Unit	**Min (-α)**	**-1_{DoE}**	**0_{DoE}**	**$+1_{DoE}$**	**Max (+α)**
x_{Nondim}	--	***-2.378***	***-1.0***	***0.0***	***+1.0***	***+2.378***
Re	--	250,000	351,422	425,000	498,578	600,000
Tu(u)	*%*	2.08	3.07	3.79	4.51	5.50
A_{Serr}/C	--	0.080	0.144	0.190	0.236	0.300
λ_{Serr}/C	--	0.050	0.122	0.175	0.228	0.300
z/H	--	-0.128	-0.054	0.000	0.054	0.128

The final aim of the experimental modelling is the ability to describe the defined experimental space by means of functions that take into accounts all of the influencing parameters (IP) of significance (Eq. 7). For this purpose, response variables (RV) have to be defined in order to act as target values of the regression functions. The coefficients are determined, depending on the chosen set of influencing parameters (IP).

This study focuses on the overall sound reduction of serrated LE compared to a baseline LE, and does not take into account any local effect at a discrete frequency. Consequently, the response variables (RV) of interest are limited to the overall sound pressure levels (OASPL) and are expected to describe the system with the necessary accuracy.

To define a sound pressure reduction, information on both, the baseline and the serrated LE, are necessary. The comparison reveals the effective reduction. However, the dependencies of the sound generation itself are also of interest because it facilitates the analysis of the influence of each case on the reduction independently. The emitted noise with a baseline LE is a function of the Reynolds number, of the turbulence intensity and of the angle of attack (Eq. 4). In case of serrated LE, additional influences of serration wavelength and amplitude must be taken into consideration (Eq. 5).

$$OASPL_{BL}[dB] = 20 \cdot log\left(\frac{\bar{p}_{BL}}{p_{ref}}\right) \rightarrow OASPL_{BL} = f\left(Re, Tu, {}^{y}/_{H}\right) \tag{4}$$

$$OASPL_{Serr}[dB] = 20 \cdot log\left(\frac{\bar{p}_{Serr}}{p_{ref}}\right) \rightarrow OASPL_{Serr} = f\left(Re, Tu, {}^{A}/_{C}, {}^{\lambda}/_{C}, {}^{y}/_{H}\right) \tag{5}$$

where $p_{ref} = 2 \cdot 10^{-5}$ Pa and the underlying frequency range $f_{Analyse}$ = 300 Hz – 10 kHz. Subtracting the $OASPL_{Serr}$ from the $OASPL_{BL}$ gives the overall sound pressure level reduction ΔOASPL, and equals the logarithmic quotient of both emitted overall sound pressures (Eq. 6).

$$\Delta OASPL[dB] = OASPL_{BL} - OASPL_{Serr} = 20 \cdot log\left({}^{\bar{p}_{BL}}/_{\bar{p}_{Serr}}\right) \tag{6}$$

3. AEROACOUSTIC MODEL

3.1 Modelling Technique

Apart from straightforward investigations regarding the absolute effect of the independent parameters on the level of broadband noise reduction, the development of a statistical-empirical model was the main objective of the present work. A crucial part of this model is the careful description of the interdependencies between the influencing parameters. For this purpose, the statistical *Design of Experiments* (DoE) approach was used, which leads to a significant reduction of the experimental volume without a relevant loss of information on the system behaviour. This approach keeps the experimental volume manageable and facilitates the detailed analysis of multiple parameters with a reasonably high accuracy. The DoE methodology was used to describe the experimental space, which is limited by the minimum and maximum levels of the five defined influencing parameters.

By using this technique, the defined response variables (RV) can be described independently by means of all influencing parameters (IP) in the first and the second order as well as the interdependencies between the influencing parameters (Eq. 7).

$$RV_i = f\left\{\sum_{j=1}^{n}\left(\left(IP_j + IP_j^2\right) + \sum\nolimits_{k=1}^{n}\left(IP_j IP_{j+k}\right)\right)\right\} \quad \begin{cases} i = 1..4 \\ j = 1..5 \\ k = 1..4 \end{cases} \tag{7}$$

The Design of Experiments methodology is based on the definition of an experimental space, consisting of a full factorial core [-1 .. +1], star points [-α .. +α] that label the upper and lower experimental boundaries, and a central point [0], defined as the experimental adjustment, where all the parameters are on their intermediary values (Table 1), (13–15). Based on this experimental composition, the analytical statistic gathers the population from a subset. A circumscribed central composite design (CCD) with pseudo-orthogonal and rotatable features was chosen as the appropriate statistical-experimental design (16). It combines the advantages of both statistical properties: orthogonality and rotatability. The trials of the strategically planned experiment were performed in a randomised order to secure the reduction or elimination of unknown and uncontrollable disturbing quantities. The analyses of the statistical significance allowed the elimination of parameters with impacts on the response variable smaller than the statistical spread.

3.2 Aeroacoustic Results

All three response variables were analysed with the previously described *Design of Experiment* methodology. Figure 3a shows the comparison of the observed and the predicted values in the case of the emitted noise from the serrated LE. The diagonal line represents the optimum in the form of a perfect match of the experimentally observed and regression-predicted values. In addition to the initially gathered data points, which were needed for the development of the model, a total of 284 extra data points were incorporated into the model in order to increase the database and thus the stability of the model. Figure 3a shows that the results of the serrated OASPL have an excellent agreement with the model, resulting in a standard deviation of 0.15 – 0.17 % and highlighting the validity to describe the system via the DoE approach.

The emitted noise with a baseline LE was analysed by varying the Reynolds number, the turbulence intensity and the angle of attack. Note that the serration amplitude and the wavelength do not affect the baseline noise prediction. The statistical spread rises slightly, however, when defining the overall noise reduction as uncertainties of the baseline and the serration prediction accumulate. For the first time, a ranking of the main factors and the interdependencies by means of their influence on the broadband noise radiation of serrated LEs is presented. The Pareto diagram in Fig. 3b shows enhancing (> 0) and damping (< 0) effects of the influencing parameters on the target values.

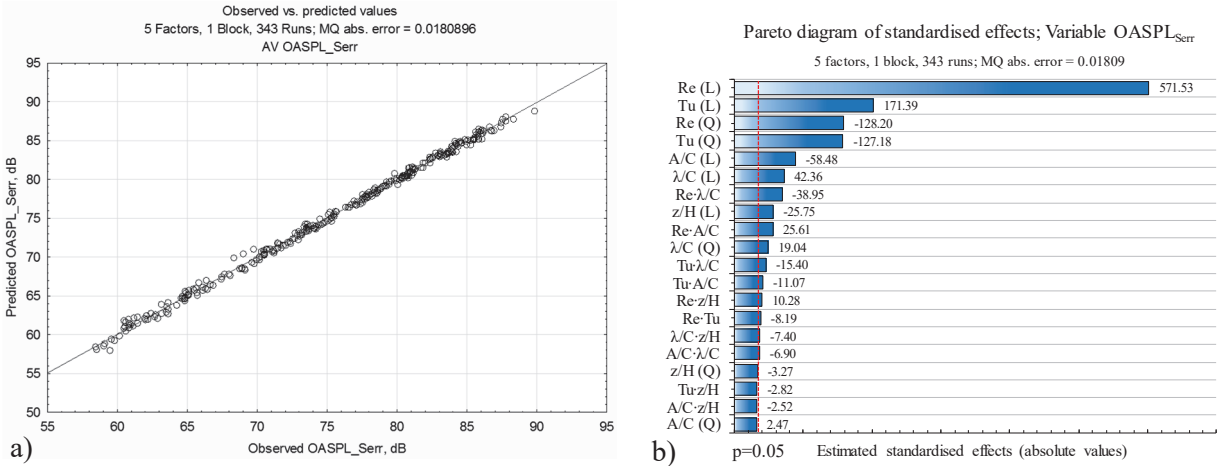

Figure 3 – a) Check of fit by plotting observed vs. predicted values of the overall sound pressure level with serrated LE ($OASPL_{Serr}$). b) Pareto diagram with ranking of enhancing (> 0) and extenuative (< 0) effects. Red line indicates level of statistical significance (p = 5 %). Distinction between linear (L) and quadratic (Q) effects.

The intermediate effects of the influencing parameters on the overall noise reduction (ΔOASPL), which characterises the sound reduction capability of the LE serrations, are plotted in Fig 4. The diagrams show that, in contrast to the response variables of the serrated noise in the absolute value of OASPL (Fig. 3b); the most dominant factor affecting the level of broadband noise reduction is the serration amplitude with a maximum of ΔOASPL = 5.3 dB (Fig. 4a), where the gradient decreases at high amplitudes. The Reynolds number, previously the strongest enhancing factor, seems to weaken the sound reduction capability (Fig. 4b). Moreover, an increased influence of the serration wavelength on the sound reduction is visible (Fig. 4c). It shows an optimum at small to intermediate values, whereas at high wavelength the noise reduction capability is weakened considerably. In general, the most significant dependencies of the overall sound pressure level reduction (ΔOASPL) are backed by findings of previous studies (1,2,6,17–22).

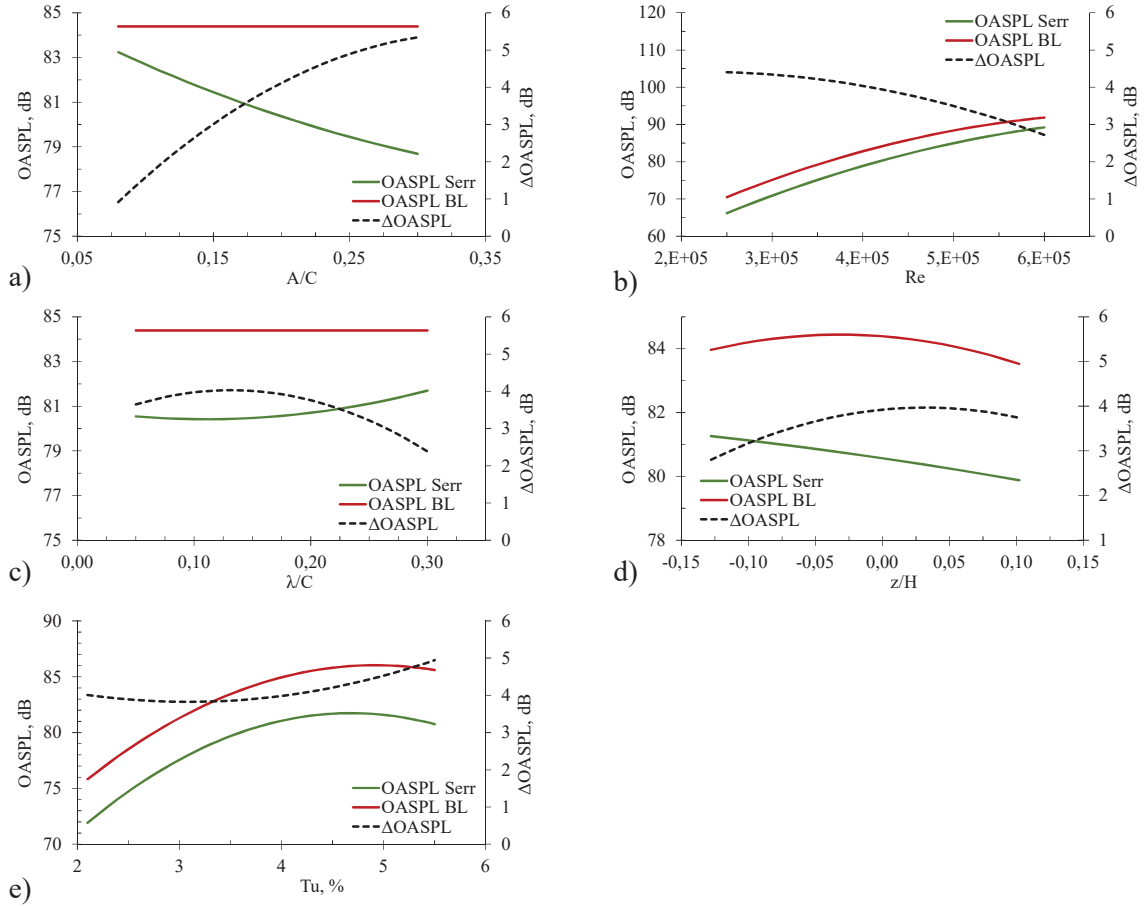

Figure 4 – Intermediate and independent influence of the analysed factors on the response variables. Disregarded influencing factors remain on intermediate levels (Re = 425,000, Tu = 3.8%, A/C = 0.19, λ/C=0.175, z/H = 0).

A remarkable effect was found to be an interdependency between the serration wavelength and the turbulence intensity (λ/C·Tu). Especially at low Tu, small serration wavelengths are crucial to achieving a high level of noise reduction, as exhibited by the red-coloured region in Fig. 5. As the Tu is related to the integral length scale Λ_{uu} of the incoming gust, large serration wavelengths are expected to reduce the de-correlation effects, if the incoming gust is characterised by small sizes of the turbulent structures. Previous investigations suggested that wavelengths that are as small as possible are beneficial for high noise reduction capability albeit the impact of the wavelength was regarded as small compared to the serration amplitude (1,2,6). The statistical DoE analysis shows that the optimal wavelength highly depends on the incoming Tu. Low to intermediate turbulence intensities back the findings of the preliminary investigations that a low serration wavelength is more desirable. However, at high Tu, wavelengths of intermediate values are far more effective in reducing the emitted OASPL, as shown in Fig. 5. This backs the finding of a recently published work, where the optimum serration wavelength is defined as twice the size of the incoming turbulent structure in the form of the integral length scale Λ_{uu} (1). An optimal set of Tu and λ/C leads to an OASPL reduction of > 5dB.

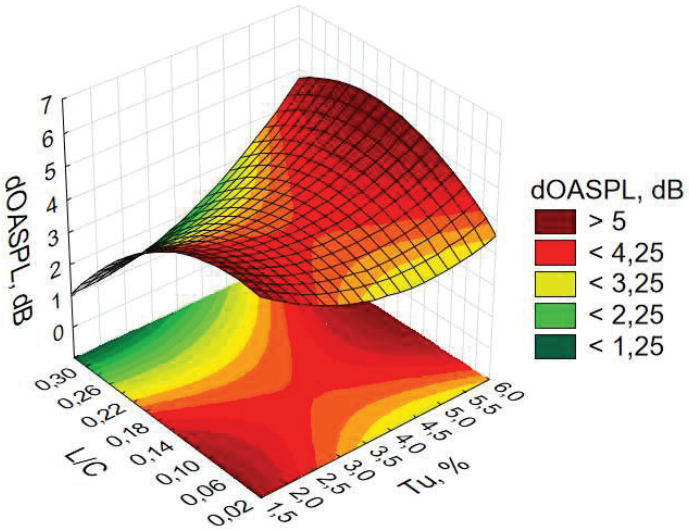

Figure 5 – Influence of interdependency between serration wavelength (L/C or λ/C) and turbulence intensity (Tu) on the OASPL reduction (ΔOASPL). Other influencing factors remain on intermediate levels (Re = 425,000, A/C = 0.19, z/H = 0).

4. FLOW VISUALISATION VIA PIV

Particle Image Velocimetry (PIV) was used to trace the movement of seeded particles, illuminated by a laser light sheet. The PIV allows a two-dimensional velocity field measurement that could compensate the lack of spatial resolution by point measurements (e.g. hot wire probe). The PIV experiments took place in the anechoic chamber of the aeroacoustic wind tunnel at *Brunel University London* (10). When the aerofoil is attached to the exit nozzle with side plates, a laser light sheet is projected upwards at 90-degrees polar angle from a platform underneath the aerofoil. If [x, y, z] denote the longitudinal, transversal and vertical directions, respectively, the laser light sheet will be in the [y, z] plane.

Polyethylene glycol (PEG) was dispersed to droplets of a diameter of 1.5 µm ≤ d ≤ 2.5 µm. The injected particles show a homogeneous distribution when reaching the measurement plane.

A CCD camera was positioned downstream at a distance of 1.3 metres of the aerofoil to trace the illuminated particles. Although the on-axis positioning of the camera is preferable, it cannot be realised due to the setup restrictions and the necessity to observe the leading edge of the aerofoil that would have been blocked by the aerofoil main body at a horizontal alignment. According to the laser pulsing frequency, the camera captured 15 double frames per second, where the time delay between each pair of frames was 3.5 µs in order to track the movement of particles in the 2 mm thick light sheet. Therefore, the real resolution in time is much higher than 15 Hz, although there is a lack of data in-between, analogue to old frequency analysers, which were not capable of real-time analysis. The velocity field of planes that stretched along the aerofoil span and height (y/z-plane) was obtained by the use of an adaptive correlation, which is based on the cross-correlation, but uses a varying interrogation area (IA), which results in a final IA of 16 x 16 pixels.

A set of five different serrations as well as the baseline LE were analysed at five distinct streamwise locations each and at zero angles of attack (AoA = 0 deg). The chosen serration amplitude (A/C) and wavelength (λ/C) cover the extremes of the previously conducted aeroacoustic study.

The post analysis of the experimental data focuses on the velocity and turbulence intensity, which are expected to be causal for the noise reduction. Note that [w] and [v] refer to the vertical and spanwise components of the velocity, respectively. In this study, the [w] velocity component was found to be the dominant parameter at regions close to the serrations where only a minor effect of the [v] component was observed. For brevity, the analysis of the PIV results thus only focuses on the [w] component of the velocity. Equation 8 shows the definition of turbulence intensity Tu(w) based on the vertical velocity [w]. Note that the local mean value of the vertical velocity $\overline{W}$ was adopted as the normalisation parameter because the streamwise velocity component [u] was not measured in the PIV experiment.

$$\Delta Tu(w) = \sqrt{w'^2}\Big/\overline{W} \tag{8}$$

The resultant velocity contours at different streamwise locations for the A45λ26 case are plotted in Fig. 6. In some cases, refraction of the laser plane occurs due to the lowermost edge of the serrations. Therefore, some parts of the image need to be cropped out for clarity. The shift of the projected aerofoil region is due to a change of perspective at different streamwise locations. At the extreme observation position (POS +15 mm); the lowermost edges of the serrations are no longer visible. The trend of the velocity in Fig. 6 shows a clear secondary motion of the fluid in front of and within the serrations.

After first entering the serration interstices (POS +2 mm), the main peak of the velocity is well beneath the LE tip, indicated by the dashed lines. Increasing the streamwise position within the serration shows a shift of the main peak upwards towards the suction side. The closer the plane is to the serration root, the higher is the influence of the serration on the fluid above the aerofoil. The results show that the region of high velocity (i.e. secondary flow) tends to expand outwards. The velocity plots also indicate that the absolute magnitude increases with the streamwise distance. This is probably due to the tendency of flow to be accelerated either upward to downward away from the serration, thus avoiding large-scale impingement to the serration root. Ultimately, both the incident surface pressure fluctuation and the scattered pressure will be reduced, resulting in broadband noise reduction. This could be the main mechanism of the noise reduction by serrations.

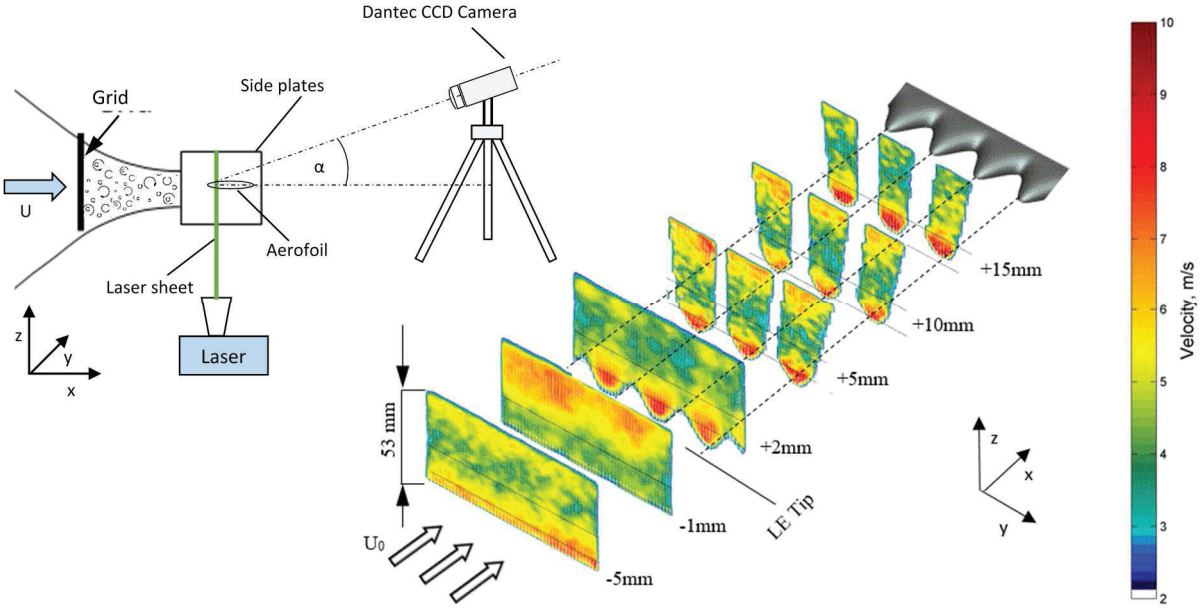

Figure 6 – Trend of vertical velocity distribution [w] along different streamwise locations by use of an A/C = 0.3, λ/C=0.175 (A45λ26) leading edge. Re = 200,000, Tu = 5.5 %, z/H = 0.

The corresponding contours of turbulence intensity Tu(w) at different streamwise locations are almost invers to the average velocity as shown in Fig. 6. In order to quantify whether a change in the mean velocity or in the velocity fluctuation is the dominant cause of a changing Tu(w) in the case of serrations, vertical profiles of the measurement data were extracted in front of the LE (Fig. 7). The comparison of the baseline and the A45λ26 serration shows a change in both the mean vertical velocity w and fluctuation w′. However, the increase of the mean vertical velocity, especially in the region of the projected aerofoil area, is more significant and reaches a maximum at the leading edge tip. On the other hand, the fluctuations remain constant in the vertical direction, and seem to show no dependency on the LE geometry. The comparison of the vertical velocity fluctuation between the baseline and serration cases in Fig. 7 indicates how significant the Tu(w) changes, even before the turbulent structures impinge on the aerofoil surface. Note that the trend of the Tu(w) at different streamwise locations should follow the same dependency, i.e. change in the Tu(w) is mostly attributed to a change in the mean vertical velocity where the vertical velocity fluctuations remain roughly constant. Therefore, regions of increased Tu(w) in the projected frontal part of the aerofoil close to the LE tip are mainly caused by the increased mean effect of large scale velocity (i.e. secondary flow) such that a direct impingement to the serration solid body is minimised, i.e. a reduced stagnation effect.

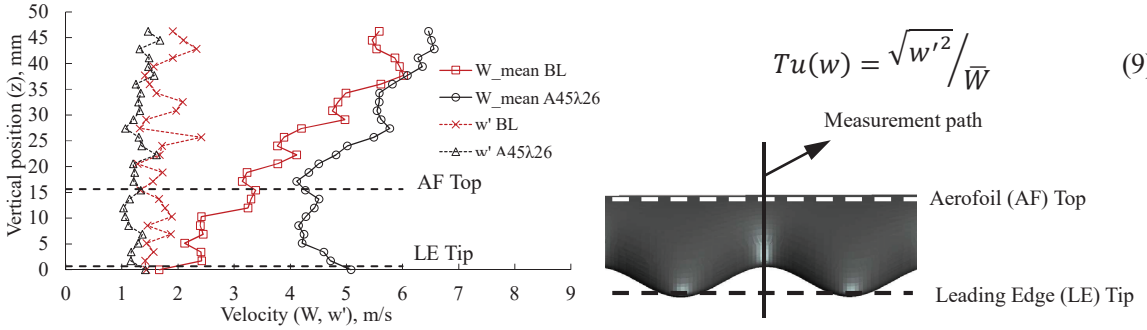

$$Tu(w) = \sqrt{w'^2}\Big/\bar{W} \tag{9}$$

Figure 7 – Vertical distribution of mean velocity $\bar{W}$ (straight) and velocity fluctuation w'^2 (dashed) at root of serration with baseline (red) and serrated leading edge (black). POS = -1mm upstream of LE tip with an A45λ26 serration. Re = 200,000, Tu = 5.5 %, A/C=0.3, λ/C=0.175.

5. NUMERICAL PERFORMANCE ANALYSIS

The developed model on the aeroacoustic performance of serrated LE in Chapter 3 clearly identified significant benefits of this application in terms of acoustics. However, LE serrations are also known to have an impact on the aerodynamic characteristics. As previous studies showed, serrations lead to slight decreases in the lift while the separation point of the aerofoil is delayed what leads to higher maximum angles of attack in the pre-stall regime. Post-stall, the serrations prevent a sharp decrease of the lift, as it is the case with straight leading edges (23–25). The aim of the current analysis is to supplement the developed aeroacoustic model with information on the aerodynamic performance of the aeroacoustically already analysed serrations. Hence, a numerical study of a cambered NACA65(12)-10 with straight (BL) and serrated leading edge (A26W45) was carried out. The incoming flow velocity was varied on 15 ms^{-1} and 60 ms^{-1} or Re=150,000 and 600,000, respectively, while the angle of attack was between $-0.256 \leq z/H \leq 0.256$ or $-20deg \leq \alpha \leq 20deg$. For the baseline case, the numerical results can be partly compared to the two dimensional *Xfoil* formulation, based on the inviscid linear-vorticity stream function panel method. Moreover, a comparison to selected experimental results is possible.

5.1 Numerical Setup & Meshing

The numerical setup consists of solving compressible RANS equations while modelling of the turbulent boundary layer took place by use of the SST turbulence model. In addition, the γ-θ-transition model was applied in order to take respect to the transition of the boundary layer from laminar to turbulent. The free stream velocity was defined at the inlet-domain while the modelled turbulence intensity was defined at the inlet as well but with the condition to match the experimental conditions and be Tu = 5% at the aerofoil leading edge. The numerical analysis were performed steady state as an extension to a transient problem showed to have no significant impact on the lift and drag performance, in particular at low angles of attack or in the pre-stall regime.

In terms of meshing, an unstructured mesh with hexahedrons and cuboids was used. The dimensions of the meshed domain were set, based on the aerofoil chord, to a multiple of 17 in the streamwise (x-wise) and a multiple of 8 in the anti-streamwise (y-wise) direction. Regarding the aerofoil surface, the chord (x-wise) was meshed with 1170 nodes/m and the span (z-wise) with 1560 nodes/m. A special care was directed to the resolution of the leading and trailing edge of the aerofoil. Starting at the aerofoil surface, an inflation layer was defined by an expansion with a constant ratio of 1.1 while the location of the first layer was set to the non-dimensional value of $0.001 < y+ < 1$ in order to guarantee precise resolving of the turbulent boundary layer via the chosen SST turbulence model (Eq. 10). u_τ is the friction velocity, ν the kinematic viscosity, τ_w the wall shear stress and ρ the fluid density.

$$y^+ = u_\tau \cdot y/\nu \quad with\ u_\tau = \left(\tau_w/\rho\right)^{1/2} \tag{10}$$

As a consequence of the chosen mesh parameters, the final mesh (Fig. 8) resulted in a total amount of $5 \cdot 10^6$ nodes for the 15 ms^{-1} case and $16 \cdot 10^6$ nodes for the 60 ms^{-1} case. Referring to mesh quality criteria, the overall maximum dihedral angle was below 160 degrees, the aspect ratio (AR) below 200 and the volume change constantly below 6. Considerations on the grid quality were supplemented by a grid and domain study in order to proof the independence of the chosen scales.

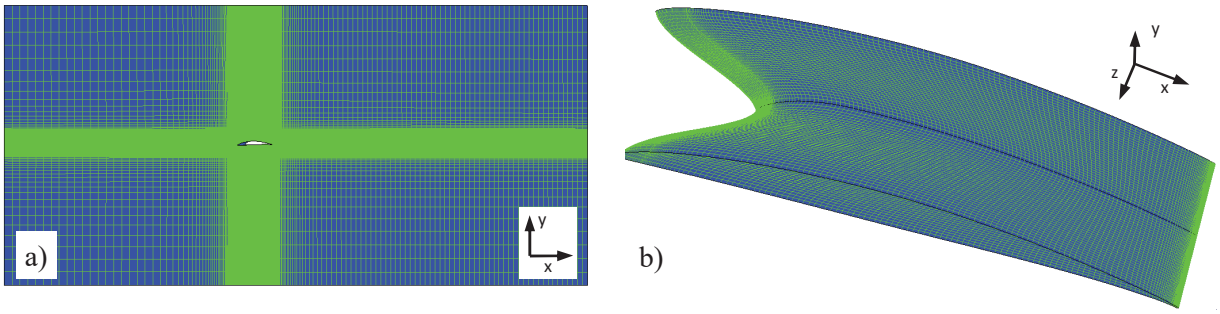

Figure 8 – Extraction of the defined mesh for the numerical study. a) full domain with visible inflation layer and position of analysed aerofoil. b) surface mesh of serrated (A26λ45) aerofoil with visible refinement of leading and trailing edge.

5.2 Aerodynamic Performance

An aerofoil with baseline and serrated LE was compared at Re=150,000 and Re=600,000 in terms of lift and drag coefficients. Assuming the flow is aligned with the z-direction, the coefficients of lift and drag are defined as shown in Eq. 11-12 where A is the effective surface area of the aerofoil. In order to enable a comparison between serrated LEs and the baseline leading edge, this area was defined to be constant as for the baseline case. Thus, for the serrated cases the real effective area is smaller compared to the one, chosen for the definition of lift and drag coefficients.

$$C_L = {2 \cdot F_L}\Big/{\rho \cdot {U_0}^2 \cdot A} \quad with \;\; F_L = F_y \cdot \cos(\alpha) - F_x \cdot sin(\alpha) \tag{11}$$

$$C_D = {2 \cdot F_D}\Big/{\rho \cdot {U_0}^2 \cdot A} \quad with \;\; F_D = F_x \cdot \cos(\alpha) + F_y \cdot \sin(\alpha) \tag{12}$$

Figure 9a shows the lift coefficients along different angles of attack (AoA). The comparison to the two-dimensional *Xfoil* panel-code exhibits a close fit while a discrepancy to experimental results occurs in particular at high AoA. This could be attributed to differences between the numerical and the experimental setup, namely to a lower experimental Tu, leading to a delayed transition of the boundary layer. Moreover, effects of limiting walls, as it is the case for the experiments, were not considered in the numerical setup. The comparison of straight (BSLN) and serrated LE in Fig. 9b shows a loss in the maximum lift of the serrated LE of up to 20%, while the effective surface area decreases by 6.3%. Thus, the decrease in effective area seems not to be the only cause for the lower lift with serrated LEs at high AoA. However, in the pre-stall region only minor changes were observed. The post-stall region of the baseline LE is more distinct while there is only a diffuse stall region for the serrated LE.

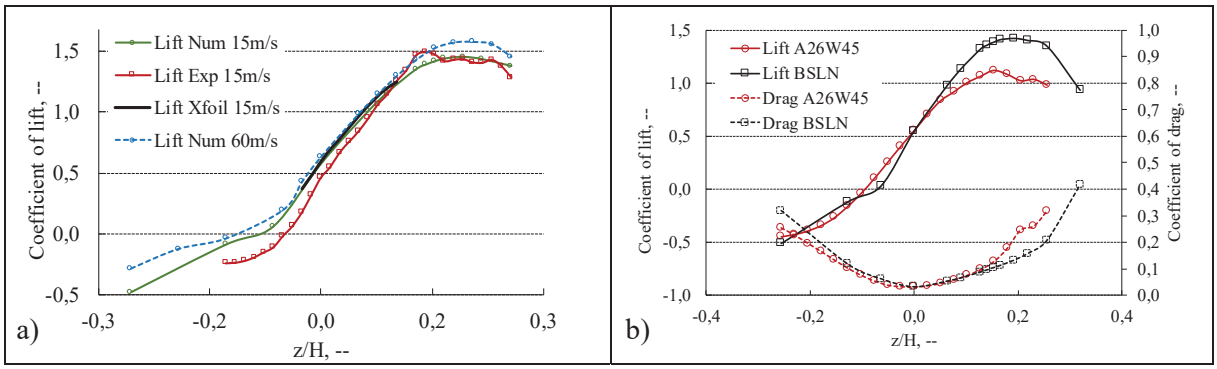

Figure 9 – a) Numerical and experimental (2) results of baseline LE at Re=150,000. Additional plot of numerical results for Re = 600,000. Tu=5% b) comparison of lift and drag coefficients with varying AoA for baseline and A26λ45 case at Re = 150,000 and Tu = 5%.

Although the serrations alter the shape of the aerofoil leading edge to a chordwise maximum of up to x/C=0.3, they show a significant effect on the pressure distribution to distances of x/C ≤ 0.45 for the pressure side and x/C ≤ 0.6 for the suction side (Fig. 10). The maximum pressure on the aerofoil suction side rises steadily in the spanwise direction from peak to trough of the serration. This spanwise pressure gradient might serve as an indicator for a spanwise secondary flow.

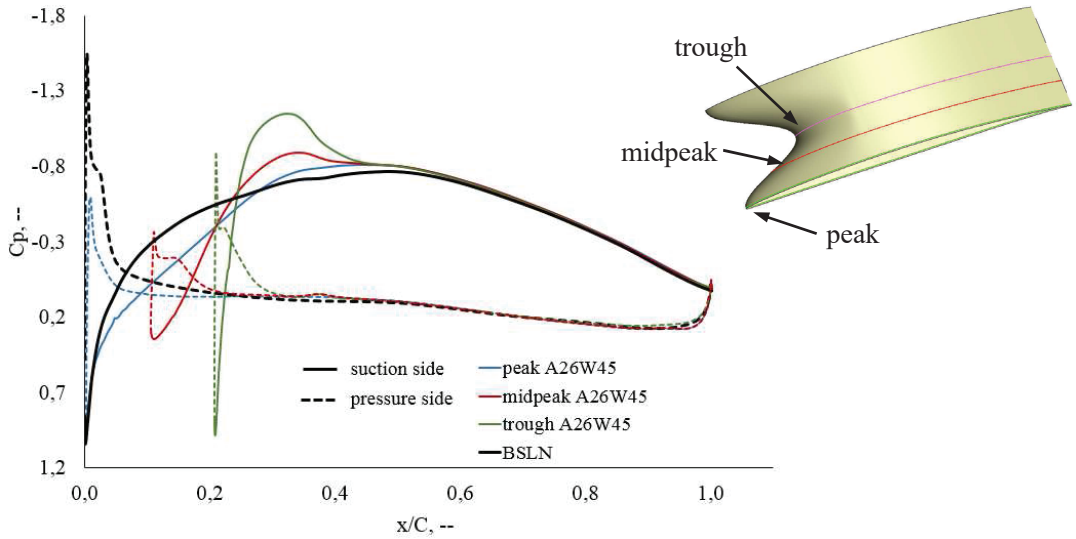

Figure 10 – Pressure distribution of A26λ45 LE at distinct spanwise locations. Additional plot of baseline case, z/H=0, Re = 150,000, Tu = 5%.

6. CONCLUSIONS

An experimental aeroacoustic study was performed in order to quantify the effects of five influencing parameters on the broadband noise emissions and reduction of a NACA65(12)-10 aerofoil with serrated leading edges. The statistical-empirical modelling technique *Design of Experiments* (DoE) was utilised to reduce the experimental volume to a manageable amount in order to gain information on interdependencies of each influencing parameter and to develop a prediction tool that describes the overall noise radiation. The model was validated and stabilised by extensive additive data. The aeroacoustic study was supplemented by Particle Image Velocimetry (PIV) experiments and a numerical study to gain insight of the flow behaviour when in close proximity or inside the serration and to enhance the knowledge on the aerodynamic performance of serrated LE. The obtained results and findings allow the current paper to reach the following conclusions:

- A clear ranking and quantification of the influencing parameters, where the Reynolds number (Re) and the freestream turbulence intensity (Tu) are the main contributors to the broadband noise emissions. The serration amplitude (A/C), followed by the Reynolds number and the serration wavelength (λ/C) represent the main factors for an effective broadband noise reduction.
- Identification of a significant interdependency of the serration wavelength and the freestream turbulence intensity (λ/C·Tu) with regard to the overall noise reduction capability. This feature could be linked to the characteristic size of the incoming gust in conjunction with a maximum phase shift.
- The effect of the stagnation point on the flow in front of the leading edge was observed to reduce drastically in the case of serrations. With an advancing streamwise position along the interstices of the serrations, the velocity (i.e. secondary flow) becomes more prominent, whilst the turbulence intensity reduces. This is regarded as the main mechanism for the reduction in broadband noise because the main flow is deflected away from the stagnation point near the serration troughs.
- The analysis of the mean vertical velocity and the vertical velocity fluctuations within the interstices of the serrations reveals that changes in the mean vertical velocity dominate the turbulence intensity Tu(w).
- Numerically obtained lift coefficients fit well to 2D theory and experimental data (post stall)
- Serrations decrease the maximum lift significantly but show a similar performance in the pre-stall region, when compared to the baseline case. In terms of the serrated LEs a discrepancy between the loss in effective area and the reduction of the lift coefficients was identified.
- An increase of the maximum pressure from peak to trough of the serrated LE is regarded as an indicator for a spanwise secondary flow.

REFERENCES

1. Chaitanya P, Narayanan S, Joseph P, Vanderwel C, Kim JW, Ganapathisubramani B. Broadband noise reduction through leading edge serrations on realistic aerofoils. 21st AIAA/CEAS Aeroacoustics Conference 2015. doi:10.2514/6.2015-2202.
2. Chong TP, Vathylakis A, McEwen A, Kemsley F, Muhammad C, Siddiqi S. Aeroacoustic and Aerodynamic Performances of an Aerofoil Subjected to Sinusoidal Leading Edges. 21st AIAA/CEAS Aeroacoustics Conference 2015. doi:10.2514/6.2015-2200.
3. Hersh AS, Sodermant PT, Hayden RE. Investigation of Acoustic Effects of Leading-Edge Serrations on Airfoils. Journal of Aircraft 1974;11(4):197. doi:10.2514/3.59219.
4. Narayanan S, Chaitanya P, Haeri S, Joseph P, Kim JW, Polacsek C. Airfoil noise reductions through leading edge serrations. Phys. Fluids 2015;27(2):25109. doi:10.1063/1.4907798.
5. Chen W, Qiao W, Wang L, Tong F, Wang X. Rod-Airfoil Interaction Noise Reduction Using Leading Edge Serrations. 21st AIAA/CEAS Aeroacoustics Conference 2015. doi:10.2514/6.2015-3264.
6. Lau AS, Haeri S, Kim JW. The effect of wavy leading edges on aerofoil–gust interaction noise. Journal of Sound and Vibration 2013;332(24):6234. doi:10.1016/j.jsv.2013.06.031.
7. Paterson RW, Amiet RK. Acoustic Radiation and Surface Pressure Characteristics of an Airfoil due to Incident Turbulence. Washington D.C., USA: United Technologies Research Center for Langley Research Center; September 1976. NASA CR-2733.
8. Staubs JK. Real Airfoil Effects on Leading Edge Noise [Ph.D. Dissertation]. Blacksburg, USA: Virginia State University; May 2008. 328 p.
9. Biedermann T, Chong TP, Kameier F. Statistical-Empirical Modelling of Aerofoil Noise Subjectedto Leading Edge Serrations and Aerodynamic Identificationof Noise Reduction Mechanisms. 22nd AIAA/CEAS Aeroacoustics Conference;2016.
10. Vathylakis A, Chong TP, Kim JH. Design of a low-noise aeroacoustic wind tunnel facility at Brunel University. In: 20th AIAA/CEAS Aeroacoustics Conference.
11. Laws EM, Livesey JL. Flow Through Screens. Annu. Rev. Fluid Mech. 1978;10(1):247. doi:10.1146/annurev.fl.10.010178.001335.
12. Rozenberg Y. Modélisation analytique du bruit aérodynamique à largebande des machines tournantes: utilisation de calculs moyennés de mécanique des fuides [Docteur Spécialité Acoustique Dissertation]. Lyon, Frankreich: L'ÉCOLE CENTRALE DE LYON; 2007.
13. Biedermann T. Aerofoil noise subjected to leading edgeserration [Master Dissertation]. Düsseldorf: Hochschule Düsseldorf; September 2015.
14. Adam M. Statistische Versuchsplanung und Auswertung (DoE Design of Experiments). 2012.
15. Clementi S, Fernandi M, Baroni M, Decastri D, Randazzo GM, Scialpi F. Mauro, A Novel Strategy for Optimizing Mixture Properties. AM 2012;03(10):1260. doi:10.4236/am.2012.330182.
16. Kleppmann W. Taschenbuch Versuchsplanung, Produkte und Prozesse optimieren. 5th ed. München: Hanser; 2008. 323 p. (Praxisreihe Qualitätswissen). ISBN: 978 3 446 41595 9. Available from: http://ebooks.ciando.com/book/index.cfm/bok_id/14235. ger.
17. Clair V, Polacsek C, Le Garrec T, Reboul G, Gruber M, Joseph P. Experimental and Numerical Investigation of Turbulence-Airfoil Noise Reduction Using Wavy Edges. AIAA Journal 2013;51(11):2695. doi:10.2514/1.J052394.
18. Gruber M. Airfoil noise reduction by edge treatments [Ph.D. Dissertation]. Southampton, UK: UNIVERSITY OF SOUTHAMPTON; February 2012.
19. Hansen KL. Effect of Leading Edge Tubercles on Airfoil Performance [Ph.D. Dissertation]. Adelaide, Australia: University of Adelaide; July 2012.
20. Narayanan S, Joseph P, Haeri S, Kim JW. Noise Reduction Studies from the Leading Edge of Serrated Flat Plates. 20th AIAA/CEAS Aeroacoustics Conference 2014. doi:10.2514/6.2014-2320.
21. Polacsek C, Reboul G, Clair V, Le Garrec T, Deniau H. Turbulence-airfoil interaction noise reduction using wavy leading edge: An experimental and numerical study. Inter Noise 2011 2011.
22. Roger M, Schram C, Santana L de. Reduction of Airfoil Turbulence-Impingement Noise by Means of Leading-Edge Serrations and/or Porous Material. 19th AIAA/CEAS Aeroacoustics Conference 2013. doi:10.2514/6.2013-2108.
23. Hansen KL, Kelso RM, Dally BB. Performance Variations of Leading-Edge Tubercles for Distinct Airfoil Profiles. AIAA Journal 2011;49(1):185. doi:10.2514/1.J050631.
24. Johari H, Henoch CW, Custodio D, Levshin A. Effects of Leading-Edge Protuberances on Airfoil Performance. AIAA Journal 2007;45(11):2634. doi:10.2514/1.28497.
25. Yoon HS, Hung PA, Jung JH, Kim MC. Effect of the wavy leading edge on hydrodynamic characteristics for flow around low aspect ratio wing. Computers & Fluids 2011;49(1):276. doi:10.1016/j.compfluid.2011.06.010.